

A near-infrared survey for new low-mass members in α Per

N. Lodieu^{1,2} *, M. J. McCaughrean^{2,3}, D. Barrado y Navascués⁴, J. Bouvier⁵, and J. R. Stauffer⁶

¹ University of Leicester, Department of Physics & Astronomy, University Road, Leicester LE1 7RH, UK
e-mail: nl141@star.le.ac.uk

² Astrophysikalisches Institut Potsdam, An der Sternwarte 16, 14482 Potsdam, Germany

³ University of Exeter, School of Physics, Stocker Road, Exeter EX4 4QL, UK
e-mail: mjm@aip.de, mjm@astro.ex.ac.uk

⁴ Laboratorio de Astrofísica Espacial y Física Fundamental, INTA, P.O. Box 50727, 28080 Madrid, Spain
e-mail: barrado@laeff.esa.es

⁵ Laboratoire d'Astrophysique, Observatoire de Grenoble, BP 53, 38041 Grenoble Cédex 09, France
e-mail: Jerome.Bouvier@obs.ujf-grenoble.fr

⁶ SIRTf Science Center, California Institute of Technology, Pasadena, CA 91125, USA
e-mail: stauffer@ipac.caltech.edu

Received November 25, 2018 /Accepted

Abstract. We present a near-infrared (K' -band) survey of 0.7 square degree area in the α Persei open cluster (age = 90 Myr, distance = 182 pc) carried out with the Omega-Prime camera on the Calar Alto 3.5-m telescope. Combining optical data (R_c and I_c) obtained with the KPNO/MOSA detector and presented in Stauffer et al. (1999) with the K' observations, a sample of new candidate members has been extracted from the optical-infrared colour-magnitude diagram. The location of these candidates in the colour-colour diagram suggests that two-thirds of them are actually reddened background giants. About 20 new candidate members with masses between 0.3 and 0.04 M_\odot are added to the ~ 400 known α Per cluster members. If they are indeed α Per members, four of the new candidates would be brown dwarfs. We discuss the advantages and drawbacks of the near-infrared survey as compared to the optical selection method. We also describe the outcome of optical spectroscopy obtained with the Twin spectrograph on the Calar Alto 3.5-m telescope for about 30 candidates, including selected members from the optical sample presented in Barrado y Navascués et al. 2002 and from our joint optical/infrared catalogue. These results argue in favour of the optical selection method for this particular cluster.

Key words. Stars: low-mass, brown dwarfs – Techniques: photometry – Techniques: spectroscopy – Infrared: stars – Hertzsprung–Russell (HR) and C–M diagrams – open clusters and associations: individual (α Persei)

1. Introduction

The bright star Alpha Persei is surrounded by a loose open cluster covering several square degrees, known as the α Per cluster. Initial cluster member selections carried out by Heckmann et al. (1956), Stauffer et al. (1985, 1989), and Prosser (1992, 1994) using proper motions, optical photometry, and radial velocity measurements revealed more than 300 cluster members (Fig. 1). They are catalogued with names starting with HE and AP for the bright and faint components, respectively. The cluster was also extensively studied in X-rays with the ROSAT satellite, confirming the membership of many photometric candidates (Randich et al. 1996; Prosser et al. 1996) and the identification of new cluster members (Prosser & Randich

1998; Prosser et al. 1998; Randich et al. 1998). Later, Basri & Martín (1999) used near-infrared photometry and spectroscopy to assess membership of candidates selected by Prosser (1994). They applied the lithium depletion test (Rebolo et al. 1992) to a handful of possible members and inferred an age for α Per of between 65 and 75 Myr, clearly rejecting three candidates and confirming the membership of two of them; the remainder were classified as probable members but lacked kinematic information. Stauffer et al. (1999; hereafter S99) applied the same lithium test to a larger sample and derived an age of 90 Myr for the cluster. S99 also added about 35 new candidate cluster members based on a combination of photometric and spectroscopic criteria. Among those new members, two objects with spectral types later than M7 were classified as brown dwarfs. Barrado y Navascués et al. (2002; ByN02) identified 54 new candidate members based on additional optical and infrared imaging, with 11 of these objects classified as candidate brown dwarf members. Based on the probable member candidates, luminosity and mass functions were derived from

Send offprint requests to: N. Lodieu

* Visiting Astronomer, German-Spanish Astronomical Centre, Calar Alto, operated by the Max-Planck-Institute for Astronomy, Heidelberg, jointly with the Spanish National Commission for Astronomy.

$0.3 M_{\odot}$ down to $0.035 M_{\odot}$ yielding a power law index α equal to 0.59 ± 0.05 (when expressed as the mass spectrum $dN/dM \propto M^{-\alpha}$), a result consistent with that obtained by different surveys of the Pleiades (Meusinger et al. 1996; Martín et al. 1998; Bouvier et al. 1998; Hambly et al. 1999; Dobbie et al. 2002; Tej et al. 2002; Moraux et al. 2003). Barrado y Navascués et al. (2004) have recently re-evaluated the age of α Per (as well as the Pleiades and IC2391), yielding 85 Myr, consistent within the errors with the S99 determination of 90 Myr. Finally, Deacon & Hambly (2004) used a pre-release of the northern hemisphere data from the SuperCOSMOS Sky Survey (Hambly et al. 2001) to identify new candidate proper motion members of α Per down to about $R = 18$ mag (corresponding to a mass of $\sim 0.15 M_{\odot}$). They also concluded that the large majority of photometrically-selected candidates in α Per and in the Pleiades have high membership probabilities.

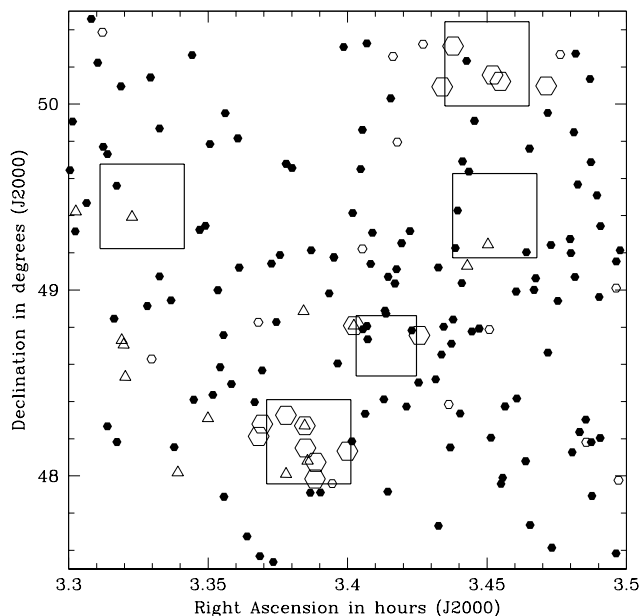


Fig. 1. Location of the known α Per members as of 2002 around the area covered with the Omega-Prime camera. Filled and open circles represent the probable and possible members, respectively, based on multi-colour photometric surveys for low-mass members in α Per. Open triangles are spectroscopically confirmed cluster members from S99. Large open hexagons are new infrared-selected candidates described in this paper. **The five Omega-Prime fields-of-view are plotted as black squares.**

As low-mass stars and brown dwarfs emit most of their flux at $1 \mu\text{m}$ and beyond, near-infrared observations should be well-suited to increase the number of cluster members and, therefore, provide a better knowledge of the cluster mass function, particularly in the substellar regime. Near-infrared ($1\text{--}2.5 \mu\text{m}$) surveys have proven an efficient way to find low-mass members and brown dwarfs in young star-forming regions, including the Trapezium Cluster (McCaughrean et al. 1995; Hillenbrand

& Carpenter 2000; Lucas & Roche 2000; Muench et al. 2001), Chamaeleon I (Comerón 2000), ρ Ophiuchus (Rieke & Rieke 1990; Preibisch et al. 2001), IC 348 (Luhman et al. 2003), Taurus-Auriga (Briceño et al. 2002), and Serpens (Kaas 1999), because low-mass stars and substellar objects are much brighter when younger. In addition, intracluster extinction due to dust hampers the detection of young objects at optical wavelengths.

Somewhat older open clusters have been surveyed extensively to probe the substellar regime, using $R\text{--}I$ and $I\text{--}z$ optical colours as a powerful discriminant to select low-mass and brown dwarf member candidates over large areas in the Pleiades (Bouvier et al. 1998; Stauffer et al. 1998; Zapatero Osorio et al. 1999; Dobbie et al. 2002; Moraux et al. 2003), σ Orionis (Béjar et al. 1999), λ Orionis (Barrado y Navascués et al. 2004), Praesepe (Pinfield et al. 1997), IC 4665 (Martín & Montes 1997), IC 2391 (Barrado y Navascués et al. 1999, 2001b; 2004), NGC 2547 (Jeffries et al. 2004), M35 (Barrado y Navascués et al. 2001a), and the α Per cluster (S99; ByN02). By extending the colour baseline, near-infrared photometry of individual candidates can be used to weed out contaminating foreground and background objects (Hodgkin et al. 1999; ByN02), and to narrow down the number of possible cluster members. Optical spectroscopy of the $H\alpha$ emission line at 6563 \AA , lithium absorption at 6708 \AA , as well as NaI and KI gravity-sensitive doublets at $7665/7699 \text{ \AA}$ and $8183/8195 \text{ \AA}$ are key features to assess the membership of low-mass candidates (Stauffer et al. 1995; Zapatero Osorio 1996). For example, the Li 6708 \AA absorption has been used to assess the substellar status of brown dwarf candidates (e.g. in σ Ori; Zapatero Osorio et al. 2002 and λ Ori; Barrado y Navascués et al. 2004), and to locate the lithium depletion boundary in various open clusters, including the the Pleiades (Stauffer et al. 1998), α Per (S99; Basri & Martín 1999), IC 2391 (Barrado y Navascués et al. 1999, 2004), and NGC 2547 (Oliveira et al. 2003; Jeffries et al. 2003).

In this paper, we present a wide-field near-infrared imaging survey (broad-band K' at $2.1 \mu\text{m}$; Wainscoat & Cowie 1992) of a 0.70 square degree area in the α Persei cluster aimed at finding new member candidates, including lower-mass brown dwarf candidates than those identified by ByN02, and at improving the knowledge of the luminosity and mass functions down into the substellar regime. By combining these new infrared data with the existing optical data from the KPNO/MOSA survey detailed in S99, we have extracted a list of ~ 100 new candidates, including new brown dwarf candidates. We assume an age of 90 Myr (S99) and a distance of $182 \pm 8 \text{ pc}$ for the cluster. Throughout, the latter is a compromise between the HIPPARCOS ($190.5^{+7.2}_{-6.7} \text{ pc}$; Robichon et al. 1999) and main-sequence fitting distances ($176.2 \pm 5.0 \text{ pc}$; Pinsonneault et al. 1998). In §2, we discuss the membership probability of the new candidates based on their location in colour-magnitude and colour-colour diagrams. In §3, we present the spectral classification of nine candidates selected from the joint optical/near-infrared catalogues. Additional spectroscopy for **optically-selected candidates (24 probable members, 1 possible, and 4 non-members)** extracted by

Table 1. Central coordinates (J2000) of the $35.4' \times 35.4'$ optical fields-of-view from S99 observed in the near-infrared, along with the observing date, exposure times, area covered, and limiting K' magnitude. The K' magnitude limit is the completeness limit defined as the point where the histogram of the number of stars per magnitude bin stops increasing. The last column provides only the range in zero points for each field of view, as there are 16 mosaics for the A, C, E, K, and L fields and 9 mosaics for the C field. Only a fraction (22–46%) of each MOSA field was covered in the near-infrared.

Field	R.A.	Dec	Obs. Date	Exp. Time	Area	K'_{complete}
A	03 27 10	+49 24	04–06 Dec 98	20 min	580 arcmin ²	17.5
C	03 24 50	+48 42	06 Dec 98	20 min	280 arcmin ²	17.5
E	03 19 35	+49 27	14 Dec 00	20 min	580 arcmin ²	15.5
K	03 27 00	+50 13	11–12 Dec 00	20 min	580 arcmin ²	17.5
L	03 23 10	+48 11	12–13 Dec 00	20 min	580 arcmin ²	17.5

ByN02, as well as for four new infrared-selected candidates, is described along with their $H\alpha$ and gravity measurements.

2. Wide-field near-infrared observations

2.1. Observations

The observations presented in this paper were carried out with the wide-field near-infrared camera Omega-Prime mounted on the Calar Alto 3.5-m telescope (Table 1) and cover a total area of 0.70 square degrees in α Per. Omega-Prime has a 1024×1024 pixel Rockwell HAWAII HgCdTe detector with a spatial scale of $0.396''/\text{pixel}$, yielding a $6.7' \times 6.7'$ field-of-view (Bizenberger et al. 1998). The first set of data was obtained on 4–6 December 1998 under good seeing ($\sim 1''$) but non-photometric conditions. Mosaics of 3×3 and 4×4 Omega-Prime fields-of-view were obtained for the A and C optical fields of S99, respectively. The second set of data was obtained on 11–14 December 2000. The seeing was variable between 1 and 1.4 arcsec with non-photometric conditions during the first three nights, and observations were made of two 4×4 mosaics in the K and L fields. The last optical field, the E field, was observed on 14 December 2000 under poorer weather conditions and is, therefore, shallower than the other fields.

Twenty exposures of 1 min each dithered by less than $40''$ around the centre of each field were obtained in order to subtract the sky and keep good signal-to-noise over the largest area possible. Differential (lights on – off) dome flat fields were taken before and after each night of observations, as well as dark frames with exposure times similar to those of our targets.

As shown in Table 1, the area covered in each field with Omega-Prime was 280 and 580 square arcmin, i.e. between 22 and 46% of the 1250 square arcmin covered in each field in the optical observations with the MOSA detector on the KPNO 4-m telescope (see S99 and ByN02 for more details).

The optical fields-of-view listed in Table 1 were observed in R_c and I_c bands with the MOSA detector mounted on the Kitt Peak 4-m telescope (see S99 and ByN02 for more details), and followed-up in the near-infrared using Omega-Prime. The mosaics observed in the infrared do not match completely the MOSA survey due to the larger optical field-of-view.

2.2. Data reduction

The observing procedure and the data reduction method were identical for both sets of infrared data. A median flat-field frame was computed each night using the tungsten-illuminated dome flats with the lights on and off. Each on-source frame was sky subtracted using the median of the remaining dithered images and divided by the flat field. Then, the individual images were aligned and stacked to create a 20 min-exposure mosaic.

Aperture photometry was carried out with a small aperture with the radius of the order of the FWHM for each detection (task *daofind* in IRAF). The flux of a few relatively bright and isolated stars was measured for different aperture sizes (from 1 to 4 times the FWHM) to compute the aperture correction. Zero point corrections to the photometry were obtained by comparison to 2MASS K_s magnitudes for stars in common with the Omega-Prime data for one or more subsections within each Omega-Prime mosaic image (typically 20 to 40 stars in each). No colour terms were applied to the photometry as no equation are available to convert K' magnitudes into the standard system. The zero points differ for all individual Omega-Prime fields-of-view and have been applied to each field. The uncertainty on the zero-points is about 0.05 mag. The completeness limit of each field is also listed in Table 1.

These limits are defined as the magnitude where the histogram of the number of stars per bin of magnitude stops increasing, a valid procedure as the great majority of sources are background field stars which should continue to increase in numbers towards fainter magnitudes. Galactic models towards the α Per cluster line of sight predict a rising luminosity function up to $K \sim 21.0$ mag (Annie Robin, personal communication). Therefore, we believe that the magnitude at which the observed luminosity stops increasing is our completeness limit and not an intrinsic feature of the field luminosity function, as it happens three magnitudes brighter than the model predictions.

2.3. Optical-infrared catalogue

Prior to the infrared survey presented in this paper, the wide-field optical survey carried out with the KPNO/MOSA detector (ByN02) had revealed ~ 100 member candidates in the α Per cluster as extracted from the $((R-I)_c, I_c)$ colour-magnitude diagram (Fig. 2). As discussed extensively in that paper, near-

infrared follow-up of the candidates in J and K had allowed us to reject some objects based on their location in optical/infrared colour-magnitude diagrams. Three subsamples were defined: 54 objects were classified as probable members; 12 as possible member candidates; and the remainder (26 objects) excluded as cluster members, implying a contamination of 25–40 %.

Initial astrometry for our K' survey was done by matching the observed coordinates (x, y) and the (RA, dec) coordinates from the USNO-A2 catalogue for three relatively bright stars available in one Omega-Prime field-of-view. After this registration, a higher number of stars (50 to 100) was used to map the field distortion in Omega-Prime, yielding RMS errors on the order of 0.1–0.2 arcsec.

We then merged our near-infrared (K') catalogue with the optical (R_c and I_c) catalogue from MOSA, using matching radius of four times the RMS dispersion values of 0.243" and 0.193" in α, δ , respectively. The final catalogue provides optical (R_c and I_c) and infrared (K') photometry for more than 22,000 stars in a 0.70 square degree area in the α Per cluster. **Only a fraction of each MOSA optical field was covered by the near-infrared observations and therefore only part of the full MOSA catalogue has been supplemented with infrared data in this study.** Table .1, available via the CDS web page, contains 22,129 entries with the following information. Columns 2 and 3 list the optical Right Ascension and declination (in J2000); Column 4 and 5 list the near-infrared Right Ascension and declination (in J2000); Columns 6, 7, and 8 give the R_c , and I_c , and K' magnitudes along with their associated errors. Column 9 provide the name for each source according to IAU convention.

2.4. Colour-magnitude diagram

The main purpose of the K' survey was to identify new cluster members, including lower mass brown dwarfs, when combined with the optical observations. Assuming an age of 90 Myr derived by the lithium depletion method (S99) and a distance of 182 pc, a 20 M_{Jup} brown dwarf in the α Per cluster has an ($I-K$) colour greater than 6 and a K magnitude of about 17.0, according to Baraffe et al. (1998) models. Therefore, the completeness limit of the K' survey is deep enough to probe the substellar regime down to 20 M_{Jup} . The optical-to-infrared colour-magnitude diagram (I_c-K', K') is shown in Fig. 3. All sources are drawn as black dots. The solid lines are the NextGen isochrones from Baraffe et al. (1998) for 50 and 100 Myr, respectively, bracketing the age of the cluster. The dotted and dashed lines are the Cond and Dusty models from Baraffe et al. (2003) and Chabrier et al. (2000), respectively. From Fig. 3, it is evident that the K -band data constitute a limit to the optical survey for the two sequences of field dwarfs. On the contrary, the optical survey represents a limit to our near-infrared survey to extract new cluster members in the α Per cluster due to the cut-off line seen from $I-K, K \sim 3.5, 19$ mag to $I-K, K \sim 6, 16.5$ mag. A similar conclusion can be drawn from Fig. 2, suggesting that our infrared survey is limited by the R_c -band observations ($R_c \leq 21.9$, $(R-I)_c \sim 2.4$). Deeper optical observations are required to check whether or not lower mass brown dwarfs

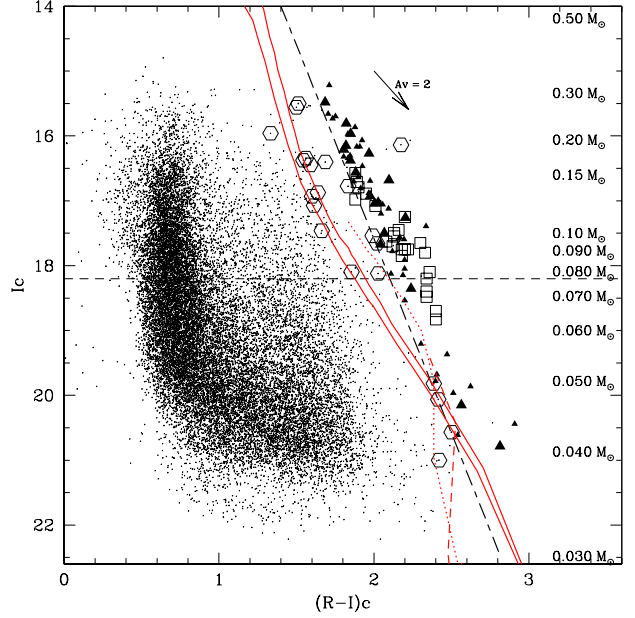


Fig. 2. Colour-magnitude ($(R-I)_c, I_c$) for all optical detections within the 0.70 square degree area surveyed in the near-infrared with the Omega-Prime camera on the Calar Alto 3.5-m telescope. Large filled triangles are probable candidates from ByN02 recovered in our optical-infrared selection whereas small filled triangles were not recovered **since the total area covered in the near-infrared was only a fraction of that covered in the optical.** Open hexagons indicate the new candidates to the right of the NextGen 100 Myr isochrones (Baraffe et al. 1998) in the optical-to-infrared colour-magnitude diagram. Open squares are spectroscopically confirmed cluster members from S99. Overplotted are the NextGen isochrones for 50 and 100 Myr (solid lines), the Cond (dotted line; Baraffe et al. 2003), and Dusty (dashed line; Chabrier et al. 2000) 100 Myr isochrones, assuming a distance of 182 pc. The fiducial cluster main-sequence used by ByN02 to select members in the optical is drawn as a short dash-long dash line. The horizontal dashed line at $I_c = 18.2$ mag indicates the stellar/substellar boundary at 0.075 M_{\odot} , assuming a distance of 182 pc and an age of 90 Myr for α Per (S99). The mass scale is indicated on the right side of the plot for the assumed age and distance using the NextGen models (Baraffe et al. 1998). **We have assumed a reddening value of $A_V = 0.30$ ($A_I = 0.179$; $A_K = 0.034$; $E(I_c-K) = 0.145$; $E(R-I_c) = 0.067$) throughout the paper, as in ByN02.**

can be extracted from the $((R-I)_c, I_c)$ colour-magnitude diagram shown in Fig. 2.

Three sequences are clearly visible in the (K', I_c-K') colour-magnitude diagram (Fig. 3). The blue side of the diagram (with $I-K < 2$) is populated on the bright end with F and G dwarfs from the Galactic thin disk, while fainter objects of this colour are primarily F and G dwarfs from the thick disk. Later type K and M dwarfs from the thin disk populate the middle colour range of the diagram ($2 < I-K < 3$).

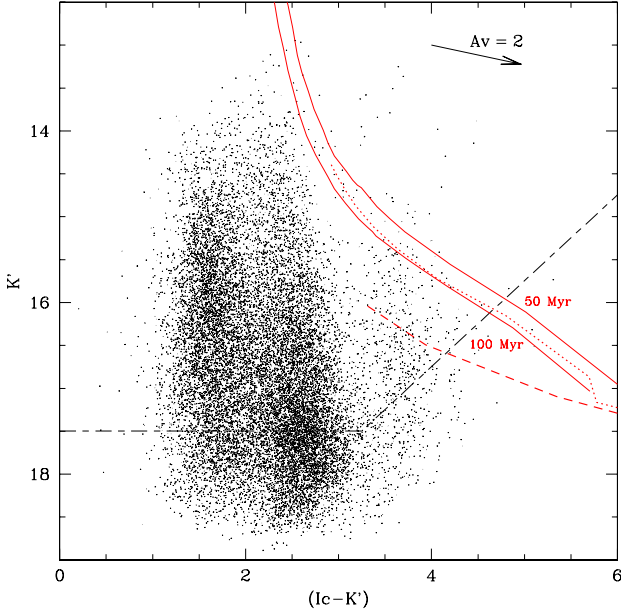


Fig. 3. Colour-magnitude (I_c-K' , K'). More than 22,000 detections are plotted as black dots. Overplotted are the NextGen isochrones from Baraffe et al. (1998) for 50 and 100 Myr (solid lines), the Cond (dotted line; Baraffe et al. 2003) and Dusty (dashed line; Chabrier et al. 2000) 100 Myr isochrones, assuming a distance of 182 pc for α Per. Our completeness limit is represented by the short dash-long dash line.

We have selected new member candidates from the optical-infrared survey by extracting objects falling to the right of the NextGen and Dusty 100 Myr isochrones (Fig. 3 and Fig. 5). As a first step, we have extracted all objects falling to the right of the NextGen 100 Myr isochrones over the whole magnitude range. The total number of newly infrared-selected candidates is 103 out of 22,129 detections in the 0.70 deg^2 surveyed area. Fig. 5 provides a close-up region of the (I_c-K' , K') colour-magnitude diagram where the new infrared-selected candidates are located. Those new cluster member candidates are represented by hexagons. We have also overplotted the optically-selected probable (filled triangles) cluster member candidates from ByN02 for comparison.

We have cross-correlated the new infrared-selected candidates with the recent release of the 2MASS database in order to provide additional J and H magnitudes. Analysis of the location of new candidates in various colour-magnitude diagrams confirmed their status as new probable members, except for AP416 which appears redder in the optical ($(R-I)_c, I_c$) colour-magnitude diagram (Fig. 2). Further analysis of the membership status of the new cluster candidates will be pursued in the next section.

As there is some evidence that low-mass brown dwarfs of age ~ 100 Myr are better traced by the Dusty models (Jameson et al. 2002), we have used those isochrones to identify a second set of low-mass α Per candidate members. Based on the optical-to-infrared colour-magnitude diagram (Figs. 3 and 5),

we have extracted about 80 new objects. Five of them remained brown dwarf candidates if they belong to the cluster; the remainder being reddened background giants as discussed in the next section. Two of the five candidates (AP399 and AP406) were previously classified as probable brown dwarf members by ByN02. The numbering of the new candidates follows from ByN02 one and starts at AP413.

2.5. Colour-colour diagram

The colour-colour diagram is of prime importance to distinguish probable cluster member candidates from distant background giants. The photometry available in three broad-band filters (R_c , I_c , K') allows us to plot a colour-colour diagram ($((R-I)_c, I_c-K')$) shown in Fig. 4. The giant branch is clearly visible and centred approximately on $(R-I)_c \sim 1$ mag and $I_c-K' \sim 3.5$ mag. A close-up of this diagram with the new infrared-selected cluster member candidates is shown in Fig. 6. The symbols used in Fig. 5 are identical to the ones used in Fig. 6. The new candidates are listed in the middle and bottom panels in Table 2.

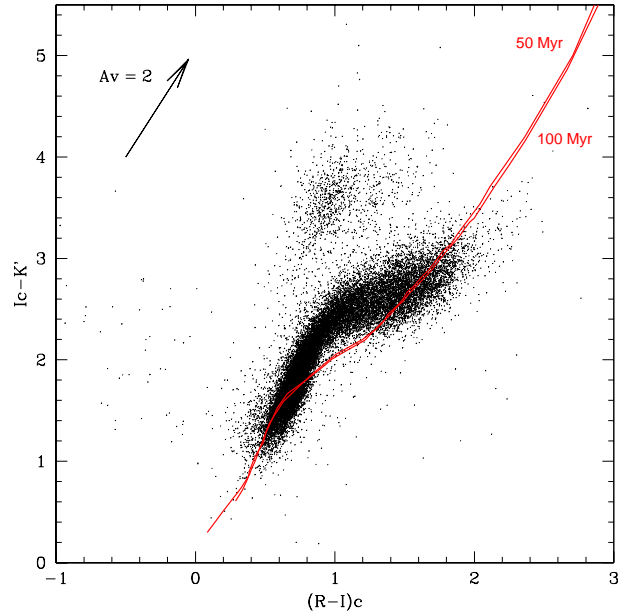


Fig. 4. Colour-colour (I_c-K' , $(R-I)_c$). Over 22,000 detections are plotted as black dots. Overplotted are the NextGen isochrones from Baraffe et al. (1998) for 50 and 100 Myr, age bracketing the one estimated for α Persei assuming a distance of 182 pc. The giant branch (roughly at $(R-I)_c \sim 1.0$ and $I_c-K' \sim 3.5$) is well populated in this diagram, showing that α Per is located towards the galactic plane.

Of the **103** infrared-selected cluster member candidates, two-thirds of them (65 %) turn out to be reddened background giants (diagonal crosses on Fig. 6 and Fig. 5) rather than low-mass brown dwarf candidates based on their location in the

Table 2. New candidate members of the α Per cluster selected from the optical-infrared survey using the NextGen and Dusty isochrones. The names, coordinates in J2000, and R_c , I_c , the 2MASS J , H , and K_s magnitudes and K' magnitudes from our near-infrared observations are quoted. The upper part of the table provides the list of 18 optically-selected member candidates found independently in the optical-to-infrared survey whereas the middle and lower parts list the new infrared-selected probable candidates. Among them, four new objects (AP430, AP431, AP432, and AP433) are brown dwarf candidate members. The numbering of the new candidate members follows the one described in ByN02 and starts at AP413.

Name	R.A.	Dec	R_c	I_c	J	H	K_s	K'
Optically-selected cluster member candidates common to our survey								
AP329	03:23:56.36	+48:09:21.1	17.16	15.48	13.88	13.31	13.04	12.95
AP332	03:25:16.91	+48:36:09.3	17.63	15.80	14.06	13.43	13.19	13.13
AP334	03:22:45.51	+48:21:33.4	17.82	15.96	14.25	13.66	13.34	13.35
AP339	03:26:33.28	+50:07:41.9	17.97	16.15	14.35	13.76	13.40	13.45
AP343	03:23:48.49	+48:36:43.3	18.01	16.21	14.62	14.07	13.72	13.66
AP344	03:26:52.11	+50:00:32.8	18.24	16.27	14.33	13.69	13.39	13.44
AP309	03:22:40.69	+48:00:33.8	18.23	16.38	14.49	13.88	13.58	13.59
AP349	03:26:48.01	+50:02:15.7	18.45	16.56	14.62	14.04	13.73	13.78
AP353	03:24:48.69	+48:49:47.3	18.78	16.68	14.61	14.00	13.65	13.63
AP364	03:20:39.19	+49:32:06.2	18.90	16.92	15.00	14.41	14.03	14.00
AP365	03:28:22.98	+49:11:24.3	19.06	17.03	15.02	14.33	14.15	14.20
AP366	03:26:35.49	+49:15:44.2	19.05	17.04	15.12	14.54	14.22	14.15
AP369	03:26:45.11	+50:25:06.7	19.46	17.26	14.88	14.26	13.88	13.84
AP311	03:23:08.70	+48:04:50.7	19.56	17.50	15.44	14.71	14.32	14.46
AP378	03:27:01.00	+49:14:41.2	19.71	17.67	15.61	14.94	14.50	14.62
AP305	03:19:21.62	+49:23:31.1	20.59	18.36	15.81	14.96	14.64	14.78
AP399	03:25:48.55	+50:01:00.8	22.71	20.15	—	—	—	16.09
AP406	03:23:09.86	+48:16:30.0	23.60	20.78	—	—	—	16.31
New infrared-selected cluster member candidates (NextGen isochrones)								
AP413	03:24:17.75	+48:07:36.0	17.01	15.50	14.03	13.34	13.05	13.06
AP414	03:22:05.17	+48:12:46.1	17.06	15.56	14.00	13.26	13.05	12.97
AP415	03:23:59.79	+48:03:57.6	17.29	15.96	14.48	13.82	13.62	13.44
AP416	03:25:32.89	+48:45:21.4	18.31	16.14	13.75	13.06	12.82	12.85
AP417	03:28:16.33	+50:05:51.6	17.91	16.34	14.57	13.91	13.63	13.63
AP418	03:23:59.92	+48:08:00.5	17.92	16.38	14.84	14.09	13.87	13.81
AP419	03:22:40.50	+48:19:35.0	18.09	16.40	14.80	14.09	13.83	13.78
AP420	03:26:02.06	+50:05:34.7	18.04	16.45	14.68	14.06	13.71	13.78
AP421	03:23:18.80	+48:04:25.4	18.61	16.77	14.75	14.07	13.77	13.87
AP422	03:27:17.27	+50:07:19.8	18.51	16.87	15.12	14.41	14.13	14.12
AP423	03:22:09.83	+48:16:43.8	18.53	16.93	15.30	14.66	14.28	14.19
AP424	03:23:17.96	+47:59:01.7	18.69	17.07	15.31	14.54	14.20	14.28
AP425	03:27:25.41	+50:05:05.4	19.12	17.46	15.61	14.79	14.56	14.51
AP426	03:24:08.12	+48:48:30.0	19.53	17.54	15.50	15.03	14.44	14.59
AP427	03:23:04.86	+48:16:11.3	19.68	17.66	14.61	15.15	14.61	14.62
AP428	03:23:05.59	+48:09:00.7	19.95	18.10	16.12	15.07	14.76	14.97
AP429	03:27:07.06	+50:09:22.7	20.15	18.12	15.75	15.00	14.77	14.78
AP430	03:26:16.24	+50:18:43.3	23.07	20.57	—	—	—	16.03
New infrared-selected cluster member candidates (Dusty isochrones)								
AP431	03:24:06.45	+48:23:11.5	22.20	19.82	—	—	—	16.07
AP432	03:27:30.59	+49:11:09.6	22.48	20.06	—	—	—	16.27
AP433	03:20:14.94	+49:31:46.6	23.42	21.00	—	—	—	16.39

$((R-I)_c, I_c-K')$ colour-colour diagram. The source of this contamination lies in the fact that the K' band probes larger distances through highly extincted regions close to the Galactic plane; α Per lies at $(l, b) = (146.5, -7.5)$. The remaining infrared-selected candidates, which are located along the Baraffe et al.

(1998) NextGen isochrones in the colour-colour diagram, remain probable cluster member candidates. However, half of these candidates (18 out of 36) were already extracted by the optical survey, thus confirming their probable membership (filled triangles in Fig. 6 and Fig. 5; upper part of Table 2). The

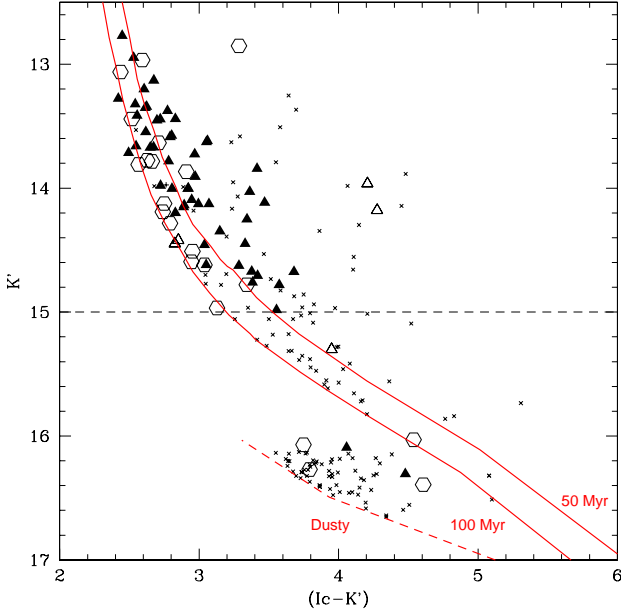


Fig. 5. Zoom of the colour-magnitude (I_c-K' , K') where the new infrared-selected member candidates are located. Overplotted are isochrones from Baraffe et al. (1998) for 50 and 100 Myr (solid lines), and the Dusty (dashed line; Chabrier et al. 2000) 100 Myr isochrones, assuming a distance of 182 pc for the cluster. Filled triangles are probable cluster member candidates extracted by the optical survey (ByN02) whereas open triangles are possible members from the same study. Open hexagons are new infrared-selected cluster member candidates from our optical-infrared survey. The diagonal crosses indicate the distant background giants. The horizontal dashed line represents the stellar/substellar boundary at $M_K = 8.3$, assuming a distance modulus of 6.3 for the cluster and an age of 90 Myr.

remaining 18 objects are new infrared-selected probable member candidates not extracted as such by the optical survey (open hexagons in Fig. 6 and Fig. 5; middle and lower part of Table 2). One of these new member candidates (AP430) has R_c , I_c , and K' magnitudes below the hydrogen-burning limit, indicating a probable brown dwarf cluster member. Another candidate (AP429) straddles the stellar/substellar boundary and is possibly a brown dwarf. Finally, AP428 lies close to the lithium depletion boundary estimated by S99.

Of the 80 cluster candidates selected to the right of the Dusty isochrones (Fig. 5), five remain brown dwarf candidates if they belong to the cluster. The other objects lie in the giant branch, as seen in galactic models (Annie Robin, personal communication). Thus, the contamination is very high in this part of the diagram, reaching over 90 %

One can now ask the following question: why were those new infrared-selected cluster member candidates missed in the optical selection? To address this issue, we have compared the location of the new candidates to previous members in the optical ($(R-I)_c$, I_c) colour-magnitude diagram (Fig. 2).

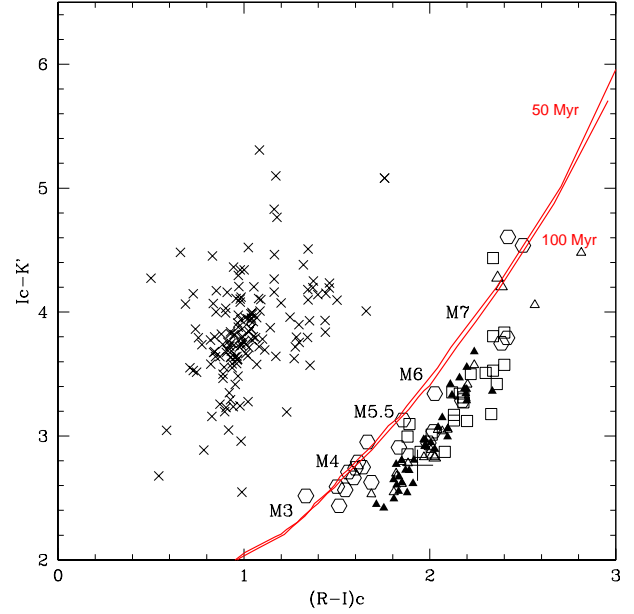


Fig. 6. Colour-colour (I_c-K' , $(R-I)_c$). Overplotted are NextGen isochrones from Baraffe et al. (1998) for 50 and 100 Myr, bracketing the age estimated for the cluster. Filled and open triangles are probable and possible member candidates extracted by the optical survey (ByN02). Open squares are spectroscopically confirmed members of α Per (S99). Open hexagons are new infrared-selected cluster member candidates from our optical-infrared survey. The diagonal crosses indicate the distant background giants rejected as cluster members. Spectral types for dwarfs from the young disk are marked (Leggett 1992).

All the infrared-selected candidates located to the right of the NextGen isochrones in the (I_c-K' , K') colour-magnitude diagram also lie to the right of the NextGen isochrones in the ($(R-I)_c$, I_c) colour-magnitude diagram. The new infrared-selected candidates define a bluer sequence than the optically-selected candidates by ~ 0.2 – 0.3 mag in the (I_c , $(R-I)_c$) colour-magnitude diagram (Fig. 2) and therefore remain likely new cluster member candidates. Some objects follow the sequence defined by the probable candidates extracted by ByN02. One object, AP415, lies below the isochrones, suggesting that it is likely a contaminant (Fig. 2). It would therefore be interesting to follow-up those new probable candidates spectroscopically to determine the cut-off line of the cluster sequence in the optical colour-magnitude diagram. It could originate from the original candidate selection procedure which made use of the Zero-Age-Main-Sequence (Leggett et al. 1992) as a criterion (ByN02). **The age of α Per is not questioned here since those objects are located on the right of the 100 Myr NextGen isochrone (Baraffe et al. 1998) in the ($(R-I)_c$, I_c) colour-magnitude diagram. The choice of the distance however affects the number of selected candidates because larger/smaller distances to the cluster would move the isochrones in the colour-magnitude diagrams. Choosing the HIPPARCOS distance of 190 pc, for example, would lead**

to the identification of two additional objects, AP418 and AP428, which are listed in Table 2. The number of objects common between the optical and the infrared selected samples did not vary, and neither did the fractional contamination.

3. Spectroscopic follow-up

3.1. Observations

Spectroscopic observations were carried out with the Twin spectrograph mounted on the Calar Alto 3.5-m telescope in October/November 2002. Weather conditions were variable over the four night observing run.

The Twin CCD camera has a 2000×800 pixel CCD detector with a spectral resolution of 1.5 \AA/pixel . We have obtained moderate-resolution ($R \sim 2000$) optical spectra of 33 selected member candidates using the red channel with the T07 grating covering $5800\text{--}8800 \text{ \AA}$. Two different slit widths, 1.5 and 2.1 arcsec, were used according to the seeing conditions. Exposure times were adjusted to take into account the brightness of the objects as well as the weather conditions.

Our sample of objects can be divided into two categories. First, a total of 29 optically-selected candidate members from ByN02 and S99 divided into four categories: 24 probable members, 1 possible member (AP350), and 4 non-members (AP327, AP336, AP338, and AP342). Second, four new infrared-selected candidates reported in this paper (AP414, AP416, AP417, and AP420).

Table 3 lists all 33 objects observed spectroscopically, their I_c magnitudes, the observing dates, and the exposure times as well as spectroscopic results which are detailed in §3.3. Most of the objects were observed several times, each exposure being shifted along the slit by ~ 100 pixels. Spectrophotometric standard stars Feige 110 (Hamuy 1992) and G191-B2B (Massey & Gronwall 1990) were observed twice each during the night to flux calibrate the spectra. Meanwhile, some template objects with known spectral types were observed with the same set-up to derive accurate spectral type classification. Dome flat fields, dark frames and He–Ar arc lamps were taken before the beginning of each night.

3.2. Data reduction

The data reduction was standard and involved subtracting an averaged bias frame and dividing by a median-combined dome flat field. Wavelength calibration was made using He and Ar lines throughout the whole wavelength range (RMS better than 0.4 \AA). Flux calibration was achieved using an averaged sensitivity function computed with several exposures of the spectrophotometric standard stars. If several spectra were obtained for one object, the resulting co-added spectrum was the median of each individual 1-D spectrum in order to remove the cosmic rays. Optical spectra of the candidates confirmed as cluster members via spectroscopy are displayed in Fig. 7.

3.3. Spectroscopy of optical candidates

3.3.1. Spectral classification

We have assigned a spectral type to each individual confirmed member with an uncertainty of half a subclass, according to the M dwarf classification schemes defined by Kirkpatrick et al. (1999) and Martín et al. (1999). We have computed several spectral indices including TiO5 (Reid et al 1995), VO-a (Kirkpatrick et al. 1999), and the PC3 index (Martín et al. 1999). The values of the three spectral indices, listed in Table 3, were generally consistent, although gravity might influence the computation of some spectral indices due to the young age of α Per compared with field dwarfs (Martín et al. 1996).

To derive a self-consistent classification and not rely solely on spectral indices, we have compared each individual target with spectra of template M dwarfs of similar spectral types, including 2MASS J2300189+121024, 2MASS J0244463+153531A&B, 2MASS J0242252+134313 (Kirkpatrick et al. 1999) and 2MASS J0435490+153720 (Gizis et al. 1999), with spectral types M4.5, M5.0, M5.5, M6.5, and M6.0, respectively. In addition, due to possible differences in telescope/instrument configurations and detector sensitivities, other comparison objects with known spectral types, including GJ251 (M3.0), LHS1417 (M4.0), LHS0168 (M5.0), LHS1326 (M6.0), and LHS0248 (M6.5) were observed with the same set-up as our targets. The three different spectral type estimates yielded consistent results with uncertainties of half a subclass and the derived spectral types are consistent with the colours and membership of the cluster.

3.3.2. Chromospheric activity

As a sign of youth, chromospheric activity is a useful criterion to ascertain the membership of selected cluster candidates. The $H\alpha$ emission line at 6563 \AA is clearly detected in *all* 24 probable candidates from ByN02 (filled hexagons in Fig. 8). The $H\alpha$ equivalent widths range from 4 to 15 \AA and are consistent with previous measurements in α Per obtained by Zapatero Osorio et al. (1996), Prosser (1992, 1994), and S99 in the M3–M6 spectral type range (open triangles in Fig. 8). However, our sample contains too few objects to probe the turnover around M3–M4 in α Per (Zapatero Osorio et al. 1996) caused by the transition from radiative to convective cores occurring at $0.3\text{--}0.2 M_\odot$, regardless of the age (D’Antona & Mazzitelli 1994).

Furthermore, the strength of the $H\alpha$ emission line in the α Per member candidates is stronger than in field dwarfs of similar spectral types, although the chromospheric activity in field M dwarfs reaches a maximum around M6–M7 (Hawley et al. 1996) and can be as high as in young magnetically active objects (Gizis et al. 2002). For the maximum of activity in young clusters, see also the compilation of the Pleiades, α Per, and IC2391 in Barrado y Navascués & Martín (2003).

Moreover, $H\alpha$ equivalent widths measured in M4–M8 cluster members in the Pleiades are typically greater than 3 \AA . Although arbitrary, the 3 \AA value reflects the lower envelope of equivalent widths in the Pleiades (Hodgkin et al. 1995), consistent with our measurements. On the side of the high level of

Table 3. List of all 33 objects observed with the red channel of the T07 grating on the Twin spectrograph at the Calar Alto 3.5-m telescope. Names, coordinates (in J2000), I_c magnitudes, observing date, exposure times, equivalent widths for $H\alpha$ at 6563 Å (negative values for emission lines), equivalent widths (in Å) for the KI and NaI doublets at 7665/7699 Å and 8183/8195 Å, respectively, are included in the table. Values obtained for three spectral indices, TiO5 (Reid et al. 1995), VO-a (Kirkpatrick et al. 1999), and PC3 (Martín et al. 1999) are given in columns 10, 11, and 12, respectively. Former (ByN02) and new (this paper) membership status as well as the spectral types (with an uncertainty of half a subclass) are provided in columns 13 and 14. The Y, Y+, Y?, and N letters stands for members, probable members, possible members, and non-members, respectively. The objects are ordered by increasing I_c magnitude.

Target	R.A.	Dec	I_c	Date	ExpT	$H\alpha$	KI	NaI	TiO5	VO-a	PC3	Member	Sp. Type
AP327	03:20:31.74	+49:39:59.6	15.06	01 Nov 02	3 × 600 s	—	—	0.38	0.985 (****)	1.984 (****)	1.109 (****)	N → N	early-M star
AP329	03:23:56.34	+48:09:21.0	15.48	31 Oct 02	1 × 1800 s	−6.5	2.0/1.3	2.1/2.4	0.390 (M4.0)	2.001 (M4.8)	1.236 (M4.7)	Y+ → Y	M4.5 ± 0.5
AP414	03:22:05.21	+48:12:46.0	15.56	03 Nov 02	3 × 600 s	—	1.9/1.7	0.4/1.2	0.518 (M2.6)	1.950 (M4.2)	1.086 (M3.7)	N	M3.5 ± 0.5
AP330	03:34:15.60	+49:58:48.0	15.66	31 Oct 02	2 × 1800 s	−10.2	2.6/1.6	2.7/3.4	0.375 (M4.2)	1.975 (M4.5)	1.240 (M4.7)	Y+ → Y	M4.5 ± 0.5
AP283	03:24:38.78	+48:17:17.1	15.70	10 Oct 02	2 × 1200 s	−4.2	2.3/1.6	2.4/2.8	0.386 (M4.0)	1.987 (M4.6)	1.232 (M4.7)	Y+ → Y	M4.5 ± 0.5
AP331	03:32:05.90	+50:05:55.0	15.73	31 Oct 02	3 × 900 s	−7.9	2.2/2.6	2.7/1.8	0.341 (M4.5)	1.973 (M4.5)	1.299 (M5.1)	Y+ → Y	M4.5 ± 0.5
AP332	03:25:16.90	+48:36:09.0	15.80	31 Oct 02	3 × 800 s	−8.2	2.8/1.9	3.3/2.5	0.319 (M4.8)	1.992 (M4.7)	1.307 (M5.2)	Y+ → Y	M4.5 ± 0.5
AP333	03:25:13.55	+50:27:33.0	15.86	31 Oct 02	3 × 800 s	−5.7	3.2/2.7	2.7/3.4	0.380 (M4.1)	1.942 (M4.1)	1.316 (M5.2)	Y+ → Y	M4.5 ± 0.5
AP335	03:28:52.96	+50:19:25.9	15.97	01 Nov 02	3 × 1500 s	−10.7	3.6/1.8	2.9/3.2	0.352 (M4.4)	1.994 (M4.7)	1.306 (M5.2)	Y+ → Y	M4.5 ± 0.5
AP336	03:31:55.30	+49:08:31.0	16.04	01 Nov 02	3 × 600 s	—	—	0.43	0.972 (****)	1.971 (****)	1.088 (****)	N → N	early-M star
AP337	03:34:07.50	+48:32:08.0	16.07	01 Nov 02	3 × 1200 s	−7.9	2.5/2.3	2.5/2.3	0.295 (M5.0)	2.006 (M4.8)	1.341 (M5.4)	Y+ → Y	M5.0 ± 0.5
AP338	03:24:52.65	+48:46:12.8	16.07	02 Nov 02	3 × 600 s	—	—	1.0	0.964 (****)	1.940 (****)	0.953 (****)	N → N	early-M star
AP416	03:25:32.90	+48:45:20.8	16.14	03 Nov 02	3 × 750 s	—	1.1/2.0	1.1/0.8	0.520 (M2.6)	1.980 (M4.5)	1.030 (M3.2)	N	M3.5 ± 0.5
AP339	03:26:33.24	+50:07:41.7	16.15	01 Nov 02	3 × 1200 s	−6.5	2.6/1.6	3.6/3.3	0.337 (M4.6)	1.982 (M4.6)	1.340 (M5.4)	Y+ → Y	M5.0 ± 0.5
AP340	03:21:34.85	+48:16:28.7	16.16	01 Nov 02	3 × 900 s	−3.8	5.4/4.6	3.6/4.3	0.276 (M5.2)	2.018 (M4.9)	1.390 (M5.7)	Y+ → Y	M5.0 ± 0.5
AP341	03:31:03.39	+50:24:41.6	16.16	01 Nov 02	3 × 750 s	−10.7	3.1/2.1	3.0/3.0	0.276 (M5.2)	1.997 (M4.7)	1.376 (M5.6)	Y+ → Y	M5.0 ± 0.5
AP344	03:26:52.00	+50:00:33.0	16.27	01 Nov 02	3 × 600 s	−10.6	3.4/2.3	3.1/3.1	0.254 (M5.5)	2.030 (M5.1)	1.392 (M5.7)	Y+ → Y	M5.5 ± 0.5
AP345	03:33:45.80	+50:08:53.0	16.30	01 Nov 02	3 × 600 s	−9.9	2.4/1.5	2.7/3.2	0.313 (M4.8)	1.995 (M4.7)	1.372 (M5.6)	Y+ → Y	M5.0 ± 0.5
AP346	03:21:30.06	+48:49:23.2	16.32	01 Nov 02	3 × 600 s	−8.3	2.7/2.1	2.5/3.5	0.327 (M4.7)	1.981 (M4.5)	1.381 (M5.6)	Y+ → Y	M5.0 ± 0.5
AP417	03:28:16.28	+50:05:51.7	16.34	02 Nov 02	3 × 1200 s	−4.8	0.9/1.0	2.3/2.3	0.520 (M2.6)	1.989 (M4.6)	1.048 (M3.4)	N	M3.5 ± 1.0
AP347	03:31:33.77	+49:52:02.1	16.34	01 Nov 02	3 × 600 s	−6.9	3.1/1.9	3.0/3.0	0.288 (M5.1)	1.962 (M4.4)	1.368 (M5.6)	Y+ → Y	M5.0 ± 0.5
AP342	03:25:39.24	+48:45:21.1	16.34	02 Nov 02	3 × 600 s	—	—	0.4	0.958 (****)	1.998 (****)	1.043 (****)	N → N	early-M star
AP309	03:22:40.65	+48:00:33.6	16.38	01 Nov 02	3 × 600 s	−4.9	2.1/1.5	2.3/1.6	0.345 (M4.5)	2.021 (M5.0)	1.336 (M5.4)	Y+ → Y	M5.0 ± 0.5
AP420	03:26:02.08	+50:05:34.5	16.45	03 Nov 02	2 × 750 s	—	—	—	0.979 (****)	1.970 (****)	0.871 (****)	N	G star
AP349	03:26:47.90	+50:02:16.0	16.56	02 Nov 02	3 × 1200 s	−9.6	2.4/2.2	3.3/3.4	0.293 (M5.0)	1.986 (M4.6)	1.373 (M5.6)	Y+ → Y	M5.5 ± 0.5
AP350	03:32:06.80	+49:25:23.0	16.57	03 Nov 02	1 × 750 s	—	—	1.0	1.017 (****)	1.996 (****)	0.913 (****)	Y? → N	early-M star
AP351	03:28:47.80	+50:02:01.0	16.64	02 Nov 02	3 × 1200 s	−7.6	2.5/2.1	3.5/3.7	0.295 (M5.0)	2.041 (M5.2)	1.322 (M5.3)	Y+ → Y	M5.0 ± 0.5
AP353	03:24:48.66	+48:49:47.0	16.68	02 Nov 02	3 × 1200 s	−9.2	3.6/2.9	3.0/3.1	0.228 (M5.7)	2.061 (M5.4)	1.476 (M6.2)	Y+ → Y	M6.0 ± 0.5
AP354	03:27:31.64	+48:53:23.3	16.69	02 Nov 02	3 × 1200 s	−11.1	3.4/2.6	2.9/3.2	0.224 (M5.8)	2.069 (M5.5)	1.458 (M6.1)	Y+ → Y	M6.0 ± 0.5
AP355	03:22:33.15	+48:47:00.3	16.70	02 Nov 02	3 × 1200 s	−9.2	2.9/2.7	3.3/3.7	0.297 (M5.0)	2.005 (M4.8)	1.344 (M5.4)	Y+ → Y	M5.0 ± 0.5
AP363	03:24:00.33	+47:55:29.7	16.88	02 Nov 02	3 × 1200 s	−14.9	3.1/2.0	3.7/4.1	0.288 (M5.1)	1.992 (M4.7)	1.400 (M5.8)	Y+ → Y	M5.5 ± 0.5
AP364	03:20:39.16	+49:32:06.0	16.92	02 Nov 02	3 × 1200 s	−8.2	2.4/2.8	3.9/4.3	0.430 (M3.6)	2.028 (M5.0)	1.390 (M5.7)	Y+ → Y	M5.5 ± 1.0
AP366	03:26:35.50	+49:15:43.8	17.04	02 Nov 02	3 × 1200 s	−10.5	3.4/2.3	3.1/3.1	0.244 (M5.6)	1.987 (M4.6)	1.417 (M5.9)	Y+ → Y	M6.0 ± 0.5

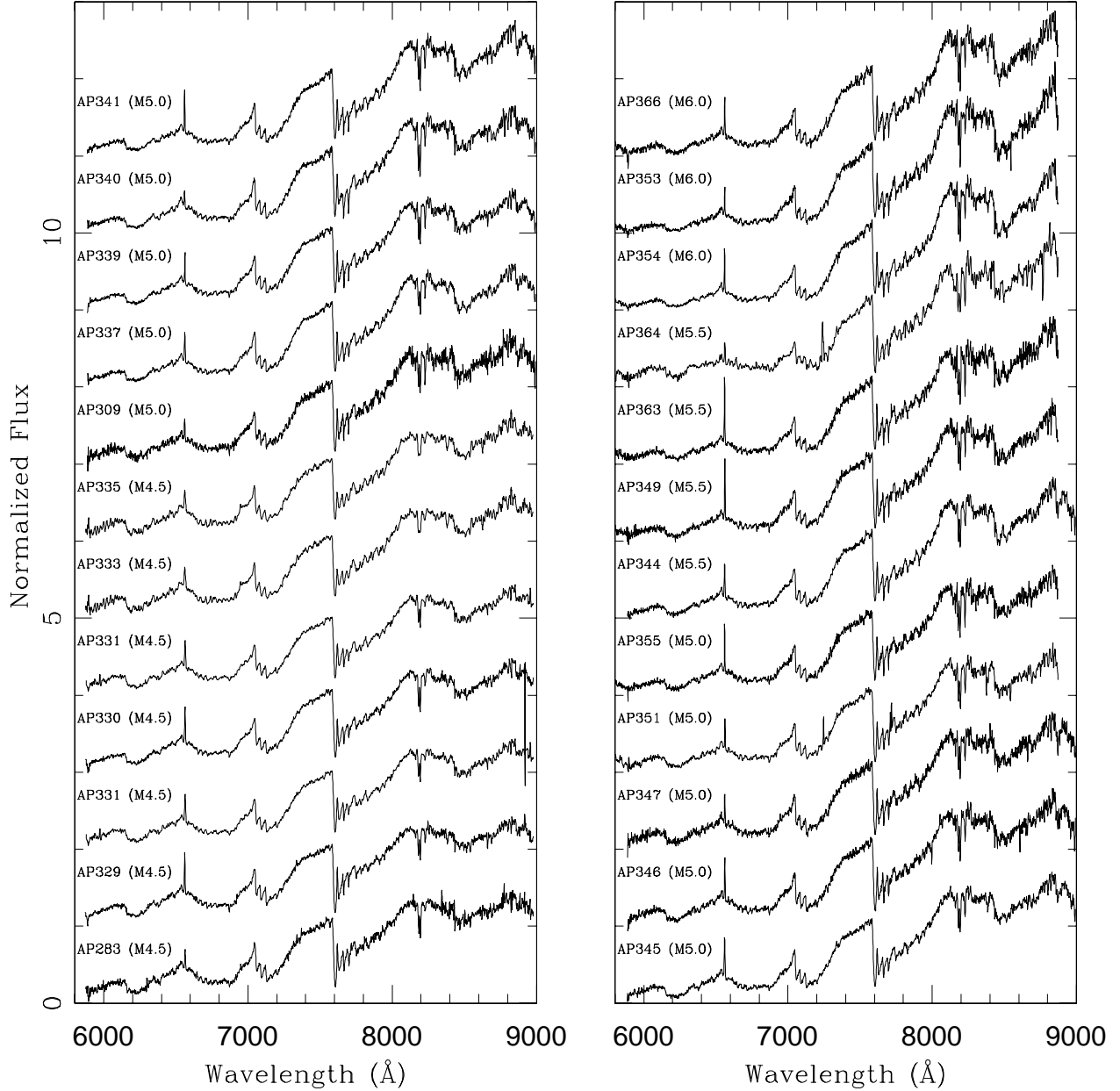


Fig. 7. Spectra of 24 objects confirmed as cluster members via optical spectroscopy. The spectral types quoted into brackets after the name of the target range from M4.5 to M6.0, with a typical uncertainty of order half a subclass. Typical features of M dwarfs are clearly seen on the spectra, including TiO and VO absorption broad bands as well as the gravity-sensitive KI and NaI doublets at 7665/7699 Å and 8183/8195 Å, respectively. All targets exhibit H α in emission at 6563 Å. An arbitrary constant has been added to each spectrum for clarity.

chromospheric activity, our findings are in agreement with the saturation limits of the H α emission line in young clusters as described by Barrado y Navascués & Martín (2003).

Therefore, the detection of the H α emission line in all probable cluster members adds support to the belief that they are indeed members of α Per.

3.3.3. Surface gravity

To further constrain the membership of the photometric candidates, we have computed the strengths of gravity-sensitive features, including the KI and NaI doublets at 7665/7699 Å and 8183/8195 Å, respectively (Table 3). The gravity decreases with younger ages, implying that young pre-main-sequence ob-

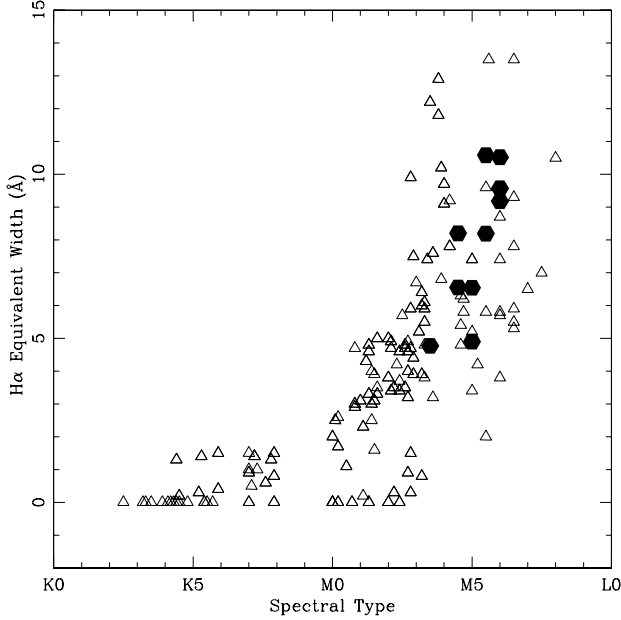


Fig. 8. $H\alpha$ equivalent widths versus spectral type for all spectroscopically confirmed cluster members in the α Per cluster. Open triangles indicate members listed in Prosser (1992, 1994) and S99. Our $H\alpha$ equivalent widths are indicated with filled hexagons and are consistent with measurements of cluster members.

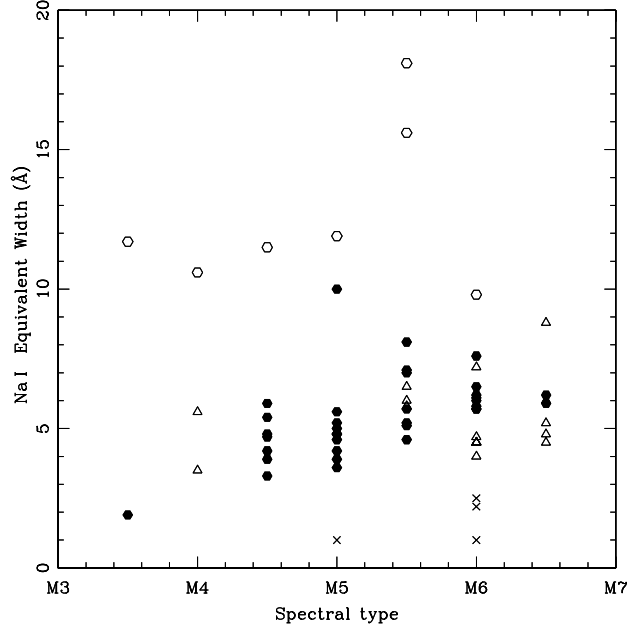


Fig. 9. Na I equivalent widths (in \AA) versus spectral type for all spectroscopically confirmed cluster members in the α Per cluster (filled hexagons). Spectroscopic data for the Pleiades (open triangles; Martín et al. 1996), σ Orionis (crosses; Béjar et al. 1999), and field dwarfs (open circles; Martín et al. 1996) are overplotted for comparison. Our measurements are compatible with those in the Pleiades, suggesting that those candidates are indeed members of α Per.

jects should harbour lower gravity and thus smaller equivalent widths.

The equivalent widths of the K I doublet in α Per are slightly smaller than for field M dwarfs of similar spectral types. Similarly, a difference in the Na I doublet equivalent widths between α Per and field dwarfs is observed, indicative of lower surface gravities (open hexagons in Fig. 9; Martín et al. 1996). The equivalent widths of the Na I doublet are on the order of 3–7 \AA , consistent with measurements in the Pleiades (open triangles in Fig. 9; Martín et al. 1996) and larger than those in σ Orionis (crosses in Fig. 9; Béjar et al. 1999). The differences are nevertheless small, as predicted: the gravity difference between 100 Myr-old cluster members and old (1–5 Gyr) field dwarfs is less than 0.2 dex according to the NextGen models (Baraffe et al. 1998).

3.4. Spectroscopy of infrared-selected candidates

We have obtained optical spectroscopy of a subsample of four infrared-selected member candidates in the α Per cluster (AP414, AP416, AP417, and AP420) to test the optical-to-infrared selection method presented in §2. We have classified those objects according to their spectral types and chromospheric activity as described below.

One object (AP420) is clearly a non-member of α Per due to its spectra exhibiting $H\alpha$ and NaID in absorption. We rejected two other candidates, AP414 and AP416, as possible members due to the non-detection of the $H\alpha$ emission line and

colours inconsistent with membership. They are likely contaminating field dwarfs with a spectral type of $M3.5 \pm 0.5$. The small overlap available between the catalogue of Deacon & Hambly (2004) and our survey shows that both objects have a membership probability lower than 60 %.

The last object, AP417, also exhibits $H\alpha$ in emission. While the equivalent width is consistent with previous studies of sources in α Per, it is on the weak side. In addition, the sequence of I_c magnitudes versus spectral type obtained for confirmed optically-selected members would predict a spectral type of M5 for this object (Table 3). However, optical spectroscopy classifies it as a significantly earlier M3.5. Therefore, we consider AP417 to be a non-member, likely a field dwarf.

In summary, the optical-infrared method presented in this paper to select cluster candidates in α Per is affected by field dwarfs and reddened objects.

4. Discussion

Our spectroscopic observations of the optically-selected candidates confirms membership in each case. All probable members exhibit $H\alpha$ in emission and have gravity measurements consistent with young objects. Those members span spectral types M4–M6, just above the M6.5 boundary which delineates the stellar/substellar border in young open clusters (Luhman 1999). Therefore, these are stellar components of the clus-

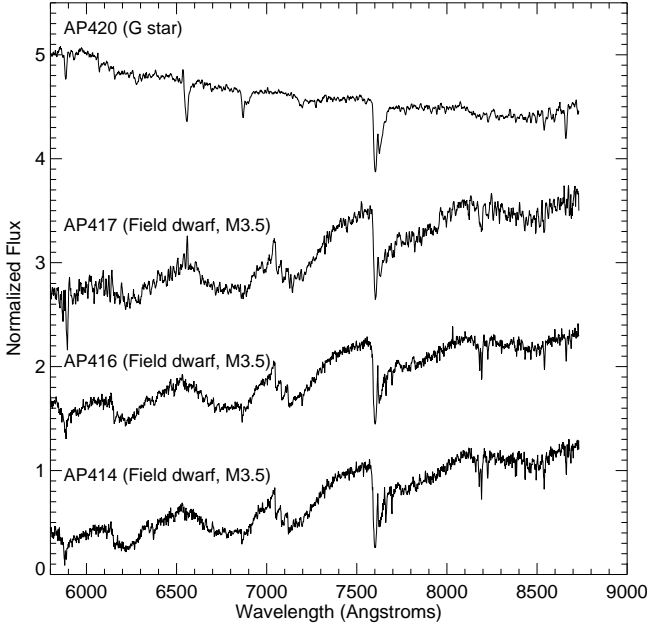


Fig. 10. Optical spectra of the infrared-selected candidates rejected as cluster members. From top to bottom are displayed the optical spectra of AP414, AP416, AP417, and AP420.

ter with masses between 0.4 and $0.12 M_{\odot}$ according to the NextGen isochrones (Baraffe et al. 1998), assuming a distance of 182 pc and an age of 90 Myr for α Per. One object, AP350, previously classified as a possible member by ByN02, was definitely rejected by our optical spectroscopy. Sources previously classified as non-members are, indeed, non-members. Hence, the original optical survey and additional near-infrared imaging follow-up appear to provide an excellent discriminant between cluster members and contaminants.

Conversely, selection based on the optical-infrared colour-magnitude diagram alone is poorer, as the contamination among selected objects is higher. The large majority of candidates selected from the (I_c-K', K') colour-magnitude diagram are reddened background giants ($\sim 70\%$). Half of the new infrared-selected candidates were previously considered as probable members while the rest await spectroscopic follow-up. In summary, the contamination of our infrared-selected sample lies in the range 70 – 85% , values higher than the estimated values from the optical survey (28 – 40% ; ByN02). In addition, none of the new infrared-selected candidates remain bona-fide cluster members after spectroscopic observations. **One of these objects, AP416, was already suspected to be a possible contaminant because it was located above the cluster sequence in Fig. 2.**

Thus, although we find the use of the K' -band a valuable tool to constrain optical selection, one should be cautious using the optical-infrared (I_c-K', K') colour-magnitude diagram as the sole criterion to extract cluster members. To find very low-mass stars and brown dwarfs, most of the surveys in the Pleiades and other open clusters are conducted in the optical (R , I , and Z) to avoid large optical-to-infrared colours such as $I-$

K , where reddened field dwarfs and distant background giants exhibit similar colours as young pre-main sequence stars.

This poses a warning for the next generation of wide-field near-infrared cameras (e.g. VISTA, WFCAM on UKIRT, WIRCam on CFHT, and Omega2000 on the Calar Alto 3.5-m telescope) being used to derive accurate mass functions down into the substellar regime in young open clusters. As an example, the UKIRT Infrared Deep Sky Survey (UKIDSS; Hambly et al. 2003) Galactic Cluster Survey (GCS) project aims to reach down to $\sim 25 M_{\text{Jup}}$ using J , H , and K broad-band filters and to survey 50 times more area in α Per than presented here. However, as we have seen the detection of low-mass stars and brown dwarfs would be optimised by including one or two optical filters (e.g. I and z) in addition to the near-infrared filters. Infrared surveys remain nevertheless very efficient in star-forming regions, where the extinction often hampers the study of low-mass members.

5. Conclusions

We have carried out a wide-field near-infrared (K' -band) survey of a 0.70 deg^2 area in the α Per cluster. Combining the new infrared photometry with existing optical (R_c and I_c) imaging, we have extracted new objects based on their location in the optical-infrared (I_c-K', K') colour-magnitude diagram. However, the position of these candidates — optical-infrared — selected in the colour-colour diagram revealed that $\sim 70\%$ of them are contaminants, including a large number of background giants due to the low galactic latitude of the cluster. Half of the remaining candidates were already identified by the optical survey of ByN02; the rest are new member candidates, including four new brown dwarfs. The optical $((R-I_c), I_c)$ colour-magnitude diagram shows that the new infrared-selected candidates define a bluer sequence than previous probable members in α Per.

We have presented moderate-resolution ($R \sim 2000$) optical (5800 – 8800 \AA) spectroscopy of 29 optically-selected candidates identified by ByN02. All probable members have spectral types, chromospheric activity, and surface gravity measurements consistent with cluster membership. They span $I_c = 15$ – 17 mag, corresponding to masses from 0.40 to $0.12 M_{\odot}$ in α Per, according to evolutionary tracks. Thus, the cluster mass spectrum derived in this mass range by ByN02 ($dN/dM \propto M^{-0.59 \pm 0.05}$) is now spectroscopically confirmed. Other candidates (possible members and likely non-members) were rejected as members on the basis of their spectra.

Finally, optical spectroscopy of four infrared-selected candidate members revealed spectral types and $H\alpha$ equivalent widths inconsistent with cluster membership. About 40 new infrared-selected candidates remain as possible cluster members, including 18 objects already classified as such by ByN02. Their optical and optical-infrared colours are consistent with membership but spectroscopic confirmation is lacking.

Acknowledgements. This work was supported by the European Commission FP5 Research Training Network “The Formation and Evolution of Young Stellar Clusters” (HPRN-CT-2000-00155) and the DFG (CA239/3-1). We are grateful to Thomas Stanke who carried

out infrared observations of the cluster in December 1998. NL thanks Richard Jameson for useful discussion on the classification of field stars. NL thanks the Calar Alto observatory staff and Gyula Szokoly for support and help during his first observing run at Calar Alto. DByN is indebted to the Spanish “Programa Ramón y Cajal” and AYA2001-1124-CO2 programs.

References

- Baraffe, I., Chabrier, G., Allard, F., & Hauschildt, P. H. 1998, *A&A*, 337, 403
- Baraffe, I., Chabrier, G., Barman, T. S., Allard, F., & Hauschildt, P. H. 2003, *A&A*, 402, 701
- Barrado y Navascués, D., Stauffer, J. R., & Patten, B. M. 1999, *ApJ*, 522, 53
- Barrado y Navascués, D., Stauffer, J. R., Bouvier, J., & Martín, E. L. 2001b, *ApJ*, 546, 1006
- Barrado y Navascués, D., Stauffer, J. R., Brice no, C., et al. 2001b, *ApJS*, 134, 103
- Barrado y Navascués, D., Zapatero Osorio, M. R., Béjar, V. J. S., et al. 2001c, *A&A*, 377, L9
- Barrado y Navascués, D., Bouvier, J., Stauffer, J. R., Lodieu, N., & McCaughrean, M. J. 2002, *A&A*, 395, 813 (ByN02)
- Barrado y Navascués, D. & Martín, E. L. 2003, *AJ*, 126, 2997
- Barrado y Navascués, D., Stauffer, J. R., Bouvier, J., Jayawardhana, R., & Cuillandre, J.-C. 2004, *ApJ*, 610, 1064
- Barrado y Navascués, D., Stauffer, J. R., & Jayawardhana, R. 2004, *ApJ*, 614, 386
- Basri, G. & Martín, E. L. 1999, *ApJ*, 510, 266
- Béjar, V. J. S., Zapatero Osorio, M. R., & Rebolo, R. 1999, *ApJ*, 521, 671
- Bizenberger, P., McCaughrean, M. J., Birk, C., Thompson, D., & Storz, C. 1998, *SPIE Proc.*, v3354, p 825
- Bouvier, J., Stauffer, J. R., Martín, E. L., et al. 1998, *A&A*, 336, 490
- Brice no, C., Luhman, K. L., Hartmann, L. et al. 2002, *ApJ*, 580, 317
- Chabrier, G., Baraffe, I., Allard, F., & Hauschildt, P. 2000, *ApJ*, 542, 464
- Comerón, F., Neuhauser, R., & Kaas, A. A. 2000, *A&A*, 359, 269
- D’Antona, F., & Mazzitelli, I. 1994, *ApJS*, 90, 467
- Deacon, N. R., & Hambly, N. C. 2004, *A&A*, 416, 125
- Dobbie, P. D., Kenyon, F., Jameson, R. F. et al. 2002, *MNRAS*, 335, 687
- Gizis, J. E., & Reid, I. N. 1999, *AJ*, 117, 508
- Gizis, J. E., Reid, I. N., & Hawley, S. L. 2002, *AJ*, 123, 3356
- Hambly, N. C., Hodgkin, S. T., Cossburn, M. R., & Jameson, R. F. 1999, *MNRAS*, 303, 835
- Hambly, N. C., Irwin, M. J., & MacGillivray, H. T. 2001, *MNRAS*, 326, 1295
- Hambly, N. C., and the UKIDSS Consortium 2003 in IAU Symposium 211, “Brown Dwarfs”, ed. E. L. Martín (San Francisco:ASP), p 477
- Hamuy, M., Walker, A. R., Suntzeff, N. B., et al. 1992, *PASP*, 104, 533
- Hawley, S. L., Gizis, J. E., & Reid, I. N. 1996, *AJ*, 112, 2799
- Heckmann, O., Dieckvoss, W., & Kox, H. 1956, *AN*, 283, 109
- Hillenbrand, L. A., & Carpenter, J. M. 2000, *ApJ*, 540, 236
- Hodgkin, S. T., Jameson, R. F., & Steele, I. A. 1995, *MNRAS*, 274, 869
- Hodgkin, S. T., Pinfield, D. J., Jameson, R. F., et al. 1999, *MNRAS*, 310, 87
- Hunt, L. K., Mannucci, F., Testi, L., et al. 1998, *AJ*, 115, 2594
- Jameson, R. F., Dobbie, P. D., Hodgkin, S. T., & Pinfield, D. J. 2002, *MNRAS*, 335, 853
- Jeffries, R. D., Oliveira, J. M., Barrado y Navascués, D., & Stauffer, J. R. 2003, *MNRAS*, 343, 1271
- Jeffries, R. D., Naylor, T., Devey, C. R., & Totten, E. J. 2004, *MNRAS*, 351, 1401
- Kaas, A. A. 1999 *AJ*, 118, 558
- Kirkpatrick, J. D., Reid, I. N., Liebert, J., et al. 1999, *ApJ*, 519, 802
- Lada, E. A., & Lada, C. J. 1995, *AJ*, 109, 1682
- Landolt, A. U. 1992, *AJ*, 104, 340
- Leggett, S. 1992, *ApJS*, 82, 351
- Lucas, P. W., & Roche, F. P. 2000, *MNRAS*, 314, 858
- Luhman, K. L. 1999, *ApJ*, 525, 466
- Luhman, K. L., Stauffer, J. R., Muench, A. A. et al. 2003, *ApJ*, 593, 1093
- Martín, E. L., Rebolo, R., & Zapatero Osorio, M. R. 1996, *ApJ*, 469, 706
- Martín, E. L., & Montes, D. 1997, *A&A*, 318, 805
- Martín, E. L., Zapatero Osorio, M. R., & Rebolo, R. 1998, *ASP Conf. Ser.* 134: Brown Dwarfs and Extrasolar Planets, ed. R. Rebolo, E. L. Martín, & M. R. Zapatero Osorio, p 507
- Martín, E. L., Delfosse, X., Basri, G., et al. 1999, *AJ*, 118, 2466
- Meusinger, H., Schilbach, E., & Souchay, J. 1996, *A&A*, 312, 83
- McCaughrean, M. J., Zinnecker, H., Rayner, J., & Stauffer, J. R. 1995, *Low-Mass Stars and Brown Dwarfs in the Trapezium Cluster*. In *ESO Workshop*, ed. C. G. Tinney (Garching: ESO), p 209
- Massey, P., & Gronwall, C. 1990, *ApJ*, 358, 344
- Moraux, E., Bouvier, J., Stauffer, J. R., & Cuillandre, J.-C. 2003, *A&A*, 400, 89
- Muench, A. A., Alvés, J., Lada, C. J., et al. 2001, *ApJ*, 558, 51
- Oliveira, J. M., Jeffries, R. D., Devey, C. R., et al. 2003, *MNRAS*, 342, 651
- Pinfield, D. J., Hodgkin, S. T., Jameson, R. F., Cossburn, M. R., & von Hippel, T. 1997, *MNRAS*, 287, 180
- Pinsonneault, M. H., Stauffer, J. R., Soderblom, D. R., et al. 1998, *ApJ*, 504, 170
- Preibisch, T., Guenther, E., & Zinnecker, H. 2001, *AJ*, 121, 1040
- Prosser, C. F. 1992, *AJ*, 103, 488
- Prosser, C. F. 1994, *AJ*, 107, 1422
- Prosser, C. F., Randich, S., Stauffer, J. R. et al. 1996, *AJ*, 112, 1570
- Prosser, C. F., & Randich, S. 1998, *AN*, 319, 201
- Prosser, C. F., Randich, S., & Simon, T. 1998, *AN*, 319, 215
- Randich, S., Schmitt, J. H. M. M., Prosser, C. F., & Stauffer, J. R. 1996, *A&A*, 305, 785
- Randich, S., Martín, E. L., Lopez, R. J. G., & Pallavicini, R. 1998, *A&A*, 333, 591
- Rebolo, R., Martín, E. L., & Magazzù, A. 1993, *ApJ*, 404, L17
- Reid, I. N., Hawley, S. L., & Gizis, J. E. 1995, *AJ*, 110, 1838
- Rieke, G. H., & Rieke, M. J. 1990, *ApJ*, 362, L21
- Robichon, N., Arenou, F., Mermilliod, J.-C., & Turon, C. 1999, *A&A*, 345, 471
- Stauffer, J. R., Hartmann, L. W., Burnham, J. N., et al. 1985, *ApJ*, 289, 247
- Stauffer, J. R., Hartmann, L. W., Jones B. F., et al. 1989, *ApJ*, 289, 247
- Stauffer, J. R., Liebert, J., Giampapa, M., et al. 1994, *AJ*, 108, 160
- Stauffer, J. R., Liebert, J., & Giampapa, M. 1995, *AJ*, 109, 298
- Stauffer, J. R., Schultz, G., & Kirkpatrick, J. D. 1998, *ApJ*, 499, 199
- Stauffer, J. R., Barrado y Navascués, D., Bouvier, J., et al. 1999, *ApJ*, 527, 219 (S99)
- Tej, A., Sahu, K. C., Chandrasekhar, T., & Ashok, N. M. 2002, *ApJ*, 578, 523
- Wainscoat, R. J., & Cowie, L. L. 1992, *AJ*, 103, 332
- Zapatero Osorio, M. R., Rebolo, R., Martín, E. L., et al. 1996, *A&A*, 305, 785
- Zapatero Osorio, M. R., Rebolo, R., Martín, E. L., et al. 1999, *A&AS*, 134, 537
- Zapatero Osorio, M. R., Béjar, V. J. S., Pavlenko, Ya., et al. 2002, *A&A*, 384, 937

Online Material

Table .1. Optical-infrared catalogue of all sources detected in the 0.70 square degree surveyed area in α Per. The total number of sources with optical and infrared photometry is 22,129. Optical and infrared coordinates (in J2000) are listed in columns 2–5. Magnitudes and their associated errors in R_c , I_c , and K' are given in columns 6–8. The last column gives the name of the object according to IAU convention.

Number	R.A. (Opt)	Dec (Opt)	R.A. (NIR)	Dec (NIR)	R_c	I_c	K'	IAU Name
1	03:28:28.13	+49:36:05.5	03:28:28.16	+49:36:05.5	19.746±0.008	18.481±0.007	16.134±0.020	AP J032828+493605
2	03:28:28.10	+49:35:46.3	03:28:28.13	+49:35:46.2	20.814±0.008	19.316±0.007	16.700±0.033	AP J032828+493546
...
22129	03:21:58.24	+47:58:28.5	03:21:58.21	+47:58:28.4	21.458±0.015	19.920±0.013	17.394±0.052	AP J032158+475828